9-2008

Electron Density and Electron Neutral Collision Frequency in the Ionosphere Using Plasma Impedance Probe Measurement

E. Spencer

S. Patra

T. Andriyas

C. Swenson

J. Ward

See next page for additional authors

Authors
E. Spencer, S. Patra, T. Andriyas, C. Swenson, J. Ward, and Aroh Barjatya

Electron density and electron neutral collision frequency in the ionosphere using plasma impedance probe measurements

E. Spencer,[1] S. Patra,[1] T. Andriyas,[1] C. Swenson,[1] J. Ward,[2] and A. Barjatya[3]

Received 20 December 2007; revised 14 April 2008; accepted 4 June 2008; published 5 September 2008.

[1] Swept Impedance Probe measurements in a sporadic E layer observed during the Sudden Atomic Layer (SAL) sounding rocket mission are analyzed to obtain absolute electron densities and electron neutral collision frequencies accurately. Three sets of upleg and downleg impedance data are selected for the analysis. Initial estimates of the plasma parameters are obtained through a least mean square fit of the measured impedance data against the analytical impedance formula $Z_B(f)$ of Balmain (1969). These initial parameters are used as a starting point to drive a finite difference computational model of an antenna immersed in a plasma called PF-FDTD. The parameters are then tuned until a close fit is obtained between the measured impedance data and the numerical impedance data calculated by the PF-FDTD simulation. The electron densities obtained from the simulation were close to those obtained from the IRI 2001 model. The electron neutral collision frequencies obtained from the more accurate PF-FDTD simulation were up to 20% lower than the values predicted by Balmain's formula. The obtained collision frequencies are also lower than the quiet time values predicted by Schunk and Nagy (2000) when used in conjunction with neutral densities and electron temperature from the Mass Spectrometer Incoherent Scatter Radar Extended-90 model.

Citation: Spencer, E., S. Patra, T. Andriyas, C. Swenson, J. Ward, and A. Barjatya (2008), Electron density and electron neutral collision frequency in the ionosphere using plasma impedance probe measurements, *J. Geophys. Res.*, *113*, A09305, doi:10.1029/2007JA013004.

1. Introduction

[2] The determination of plasma parameters such as electron density and electron neutral collision frequency are important for ionospheric plasma characterization. Electron densities and density gradients are used to determine ionospheric plasma properties while the electron neutral collision frequency ν_{en}, particularly the ratio of the electron neutral collision frequency to the electron cyclotron frequency f_{ce}, is used to determine the dominant ionospheric conductivities and energy conversion processes at different ionospheric latitudes [*Heelis*, 2004].

[3] Radio Frequency probe techniques for the determination of plasma parameters are attractive especially because the RF response is not susceptible to spacecraft charging problems at frequencies above the electron plasma frequency [*Oliver et al.*, 1973], where ion sheath effects are negligible. Swept Impedance Probes in dipole configurations have been used on sounding rocket missions [*Barjatya and Swenson*, 2006] to obtain plasma electron densities in the ionospheric E and F layers. Spherical impedance probes have been used in laboratory settings [*Blackwell et al.*, 2005a, 2005b] under different bias conditions to evaluate absolute electron density. Measurements of dipole antenna impedance in a magnetized plasma with high electron densities (10^7–10^{10} cm^{-3}) and low collision frequencies have also been reported recently by *Blackwell et al.* [2007].

[4] The Swept Impedance Probe (SIP) measures the small signal RF impedance of an electrically short dipole antenna immersed in a plasma by sweeping a sinusoidal voltage over a range of frequencies and measuring the resulting current at the terminals. The measured impedance as a function of frequency is characterized by distinct resonant regions that are related to the plasma frequency f_{pe}, the electron cyclotron frequency f_{ce}, and the upper hybrid frequency f_{uh}. These resonant regions are approximately analogous to the resonances of series and parallel RLC circuits. The impedance of the antenna in a plasma is normalized by dividing it with its impedance under free space conditions, which is capacitive at wavelengths much longer than the antenna dimensions.

[5] On the normalized impedance magnitude curve of a dipole antenna immersed in a cold magnetoplasma, the

[1]Center for Space Engineering, Utah State University, Logan, Utah, USA.
[2]Computer and Electronics Engineering Technology Department, Weber State University, Ogden, Utah, USA.
[3]Physical Sciences Department, Embry Riddle Aeronautical University, Daytona Beach, Florida, USA.

0148-0227/08/2007JA013004

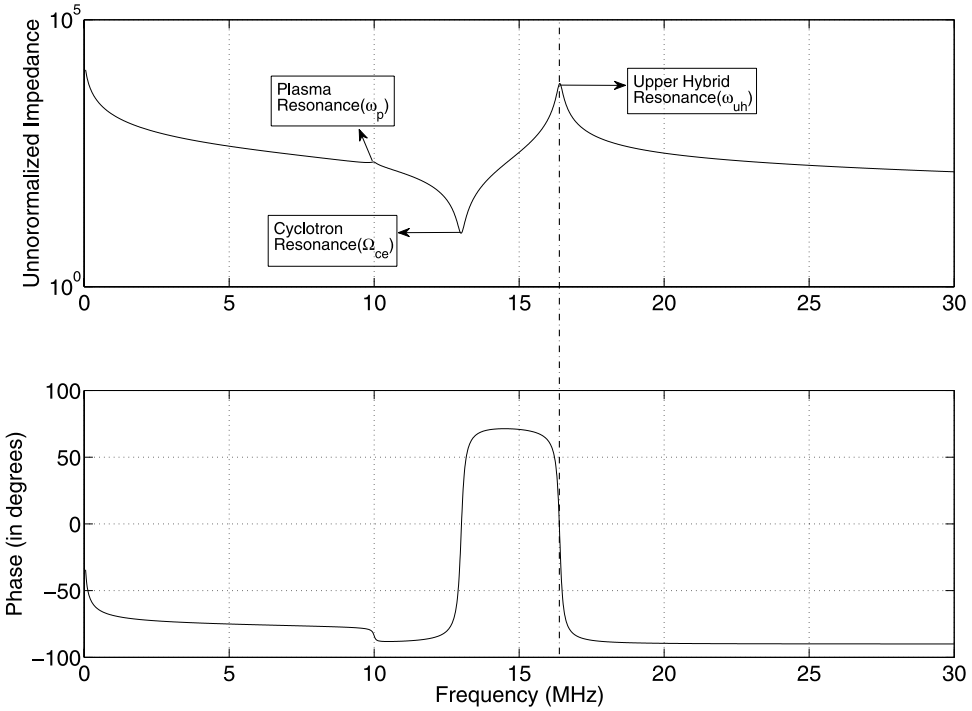

Figure 1. Unnormalized impedance magnitude and phase of a dipole antenna in a cold magnetoplasma using the Balmain formula $Z_B(f)$ showing the key resonance regions and phase transitions.

series resonance that occurs near f_{ce} gives the minimum impedance magnitude, while the parallel resonance that occurs near f_{uh} gives a local maximum in the impedance magnitude. The impedance curve for a particular combination of f_{pe}, f_{ce} and ν_{en} is unique. In a highly ionized, low collisional plasma, the parallel resonance coincides with a zero crossing in the impedance phase. The determination of the zero crossing has been used in another device known as the Plasma Frequency Probe (PFP) [*Carlson*, 2004]. The PFP uses phase locked loop principles and circuitry to track the zero phase point during sounding rocket missions. This device usually makes use of the same antenna structure as the SIP, so the measurement system alternates between the two techniques periodically. In Figure 1 an unnormalized impedance magnitude and phase curve is shown to illustrate the resonances in the magnitude and the zero phase corresponding to the parallel resonance.

[6] While the measurement technique is fairly well developed [*Carlson et al.*, 2003; *Rowland et al.*, 2006], the interpretation of the impedance data poses challenging problems. Identification of the resonant peaks and zero phase location from the impedance curves makes it possible to determine the ambient plasma electron density n_{0e} fairly well. However, the relative height and shape of the series resonance troughs and parallel resonance peaks can be interpreted to determine the electron neutral collision frequency ν_{en}. The measured data is normally compared to analytical formulas for the impedance obtained through mathematical techniques. The most popular analytical theory for a short dipole antenna immersed in a magnetized plasma is that of *Balmain* [1964] and later *Balmain* [1969]. The analytical results published by Balmain and others [*Sawaya et al.*, 1978; *Staras*, 1964; *Bishop and Baker*, 1972] have been used to fit the measured impedance curves with varying degrees of success. The major weakness of the analytical theories are that they do not self-consistently calculate the current distribution along the dipole. This results in the analytical formulas shifting the location of the resonant frequencies slightly, but more importantly, over-estimating the electron neutral collision frequencies [*Rao and Bhat*, 1969]. The formula of *Balmain* [1979] also over-estimates the free space capacitance C_0 of the dipole antenna.

[7] *Nikitin and Swenson* [2001] argue that the assumed current distribution has very little effect on the general shape of the impedance curve, but do not account for the change in the current distribution near the resonant frequencies [*Ward et al.*, 2005]. Recently *Ward* [2006] has developed a full-wave Plasma-Fluid Finite-Difference Time Domain electromagnetic code called PF-FDTD that simulates the behavior of a short dipole antenna in a magnetized plasma. The code incorporates the electron continuity and momentum equations to model the plasma environment. The PF-FDTD code computes the current distribution on the antenna structure self-consistently, thus providing a more accurate model for analysis of the measured impedance.

[8] In this work we obtain the absolute electron density and electron neutral collision frequency through analysis of impedance data from the Sudden Atomic Layer (SAL) sounding rocket experiment at different altitudes. The measured data is compared to the analytical formula $Z_B(f)$ of *Balmain* [1969] to obtain initial estimates of n_{0e}, the ambient magnetic field $\mathbf{B}_0$ and ν_{en}. The initial estimates are then used as starting values for the PF-FDTD simulation. The values are then tuned to obtain three numerical fits

to the instrument impedance data that yield upper and lower bounds on the derived parameters.

[9] In the next section we give some background of the SAL mission. Next, we discuss the PF-FDTD simulation and contrast its performance with the analytical formula $Z_B(f)$. In section 3 we describe the SIP instrument and the selected data sets. Following this we present the results of our analysis of the SAL impedance data with the PF-FDTD simulation. In section 6 we compare our results to those of the standard models. Finally we draw some conclusions and motivate further work.

2. SAL Mission Background

[10] The Sudden Atomic Layer (SAL) sounding rocket was launched from a temporary rocket range at Tortugeuro Beach, Puerto Rico on the evening of 19 February 1998, at 20:09:02 LT. The overall science objective of the SAL rocket mission was in-situ measurement of ionospheric and atmospheric conditions during a sporadic sodium (Na_s) layer event [*Gelinas*, 1999]. These Na_s layers are known to be correlated to the sporadic E (E_s) layers. The rocket flew through a neutral background sodium layer stretching from 80 km to 105 km altitude containing thin Na_s layers at 94 km and 97 km, with peak sodium densities of 6000 cm^{-3} and 4000 cm^{-3} respectively.

[11] The payload instruments included a charged dust detector to measure mesospheric dust over a mass range of 1000–10,000 amu, a Langmuir probe operating as a Fast Temperature Probe to measure the plasma density and electron temperature, Plasma Impedance (PIP) and DC probes to measure absolute and relative electron densities, electric field booms to measure fields from DC to 5 kHz, telescopes to measure sodium airglow, photometers and lamps to measure sodium and potassium densities, and a positive ion mass spectrometer. At the time of the rocket launch, two ionization layers were present, an intermediate layer at approximately 115 km and an E_s layer at approximately 92.5 km.

[12] We selected three SIP sweeps on the upleg and three on the downleg between 92 to 93 km within the E_s layer to analyze. Although the electron density can be estimated using Balmain's formula for plasma frequencies at 100 kHz and above, these sweeps were selected because the plasma densities were high enough to produce prominent resonance peaks in the impedance magnitude curves and avoid any error in estimation of ν_{en} caused by insufficient coupling at low densities [*Carlson*, 2004].

3. Plasma Impedance Probe Instrument and Data

[13] The Plasma Impedance Probe (PIP) in the SAL payload operated in two modes, a Plasma Frequency Probe mode (PFP), and the Swept Impedance Probe mode (SIP). In the SIP mode, the instrument produces an impedance curve by applying a known sinusoidal voltage across the antenna terminals and sweeping across frequencies while measuring the current into the antenna terminals. In the PFP mode, the instrument attempts to lock onto the plasma upper hybrid resonance frequency f_{uh} where the current and the voltage at the antenna terminals are in phase. When locked the PFP provides a measure of the ambient electron density n_{0e} through the relations

$$f_{pe}^2 = f_{uh}^2 - f_{ce}^2 \tag{1}$$

$$n_{0e} = \left(\frac{4\pi^2 m_e \epsilon_0}{e^2}\right) f_{pe}^2 \tag{2}$$

where e is the electron charge, and m_e is the mass of an electron. The electron cyclotron frequency f_{ce} is derived from magnetometer readings or the IGRF (International Geomagnetic Reference Field) model. The SIP operates as a network analyzer, whereas the PFP is a phase locked loop system that tracks the zero phase point associated with the upper hybrid resonance frequency f_{uh}. The SAL PIP was designed to alternate between the two modes. It could either track the parallel resonance associated with the upper hybrid frequency f_{uh} of the plasma or make sweeping impedance measurements whenever the phase transition point was undetectable because of very high collisional damping or extremely low plasma densities. The PIP consisted of two booms deployed 180 degrees apart with a 2-m tip-to-tip length and a 2.54 cm diameter. The instrument used the last 52.5 cm of the booms as active elements.

[14] The SIP swept over 40 fixed frequencies starting from 200 kHz to 12 MHz. The frequency resolution of each sweep was 50 kHz from (0.9–1.7) MHz, 100 kHz from (0.2–0.9) MHz and (1.7–2.5) MHz, 500 kHz from (2.5–4.0) MHz, 1 MHz from (4.0–6.0) MHz, and 2 MHz from (6.0–12.0) MHz. The impedance magnitude resolution was approximately 12 Ω over a range of 200 kΩ. During the SAL flight the instrument never switched to the parallel resonance tracking mode (PFP mode) and the data set consisted entirely of swept impedance magnitude measurements, at the rate of 96 sweeps per second. The response of the plasma surrounding the antenna as a function of frequency was calculated as the ratio of the measured impedance in the plasma regions above 88 km altitude to the averaged impedance at altitudes below 75.5 km where the ionization was negligible.

[15] The selected altitudes for analysis with the PF-FDTD simulation are shown in the plasma frequency profile plots of Figure 2 for the upleg and downleg of the flight. The profiles in the figure are proportional to the electron density and were generated following the technique used by *Barjatya and Swenson* [2006]. Balmain's impedance function $Z_B(f)$ was used to find a coarse fit using least mean squares technique against the measured impedance probe data $Z_m(f)$.

[16] $Z_B(f)$ gives the antenna impedance as function of five parameters, f_{pe}, f_{ce}, ν_{en}, the angle with respect to magnetic field θ, and the ion sheath size S. For the coarse fit analysis, only f_{pe} was allowed to vary. The other parameters were estimated using standard reference models. The values of f_{ce} were obtained from the IGRF model. The electron neutral collision frequencies ν_{en} were obtained by using the electron momentum transfer collision frequency formulas from *Schunk and Nagy* [2000] and neutral densities from the Mass Spectrometer Incoherent Scatter Radar Extended (MSISE)-90 model.

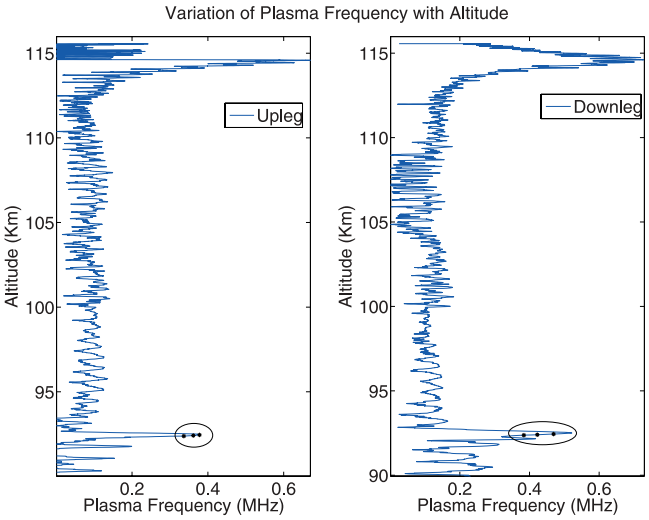

Figure 2. Upleg and downleg plasma frequency profiles obtained through a least square fit of Z_B against Z_m. The profiles are proportional to electron density through (2).

[17] At frequencies higher than the upper hybrid resonance the effects of sheath resonance and angle to the magnetic field do not play an important role [*Barjatya and Swenson*, 2006], thus θ and S were set to zero for the coarse fit.

[18] From Figure 2 we see that the SAL rocket flew through two distinct layers of high plasma density. The modulation in the derived electron density at the rocket spin rate of 1 Hz can also be observed. Three altitudes, 92.37 km, 92.41 km, and 92.44 km were chosen for the upleg analysis. The selected altitudes are shown in the figure as marks on the altitude profile enclosed by an ellipse. At these altitudes the electron density increases with increasing altitude as can be seen in Figure 2.

[19] For the downleg analysis, the three altitudes chosen were 92.38 km, 92.41 km, and 92.44 km. These are also shown in Figure 2 enclosed by an ellipse. An upward trend of electron density with increasing altitude is also noted in this case.

4. Plasma Impedance Probe Simulation

[20] A multi-species Plasma-Fluid Finite Difference Time Domain Simulation of an antenna immersed in a plasma has been developed at Utah State University under a NASA Grant (NAG5-13026) [*Ward*, 2006]. The simulation solves for the electromagnetic fields, fluid densities and fluid velocities for each plasma species around a dipole antenna self-consistently using an explicit leapfrog finite difference time domain scheme originally developed by *Yee* [1966] and later modified by others [*Taflove and Hagness*, 2005].

[21] The antenna is enclosed by a numerical bounding box that provides retarded time absorbing boundary conditions for the electromagnetic field. The electromagnetic fields are numerically solved using the Maxwell curl relations, and each plasma species density n_s and velocity $\mathbf{u}_s$ throughout the computation domain is calculated using the fluid continuity and momentum equations. Ambient density gradients over the extent of the antenna are neglected. The fluid equations are linearized to the first order, to solve only for the electromagnetic and plasma wave disturbances.

[22] The software is capable of simulating the behavior of a multi-species plasma, but here the ions and neutrals have been assumed to be stationary. The multi-fluid equations are particularized to solve only for the perturbed electron density and electron momentum in the computation domain. The simulation includes the pressure gradient $-\nabla p_e = -\nabla(n_e k_b T_e)$, but for ionospheric plasmas in typical rocket missions the cold plasma approximation can be used, so we set $T_e = 0$. Here k_b is the Boltzmann's constant.

[23] The fluid momentum and continuity equations that are analyzed in the PF-FDTD simulation are given by,

$$\frac{\partial n_e}{\partial t} = -n_{0e}(\nabla \cdot \mathbf{u}_e) \tag{3}$$

$$m_e n_{0e} \frac{\partial \mathbf{u}_e}{\partial t} = n_{0e} q_e (\mathbf{E} + \mathbf{u}_e \times \mathbf{B}_0) - n_{0e} m_e \nu_{en} \mathbf{u}_e \tag{4}$$

where, n_{0e} is the background density, n_e is the first-order density variation, u_e is the first-order velocity perturbation, and ν_{en} is the electron neutral collision frequency. The ambient magnetic field strength is given by $\mathbf{B}_0$. These two equations for the electron species fluid are supplemented by the Maxwell equations,

$$\nabla \times \mathbf{E} = -\frac{\partial \mathbf{B}}{\partial t} \tag{5}$$

$$\nabla \times \mathbf{B} = \epsilon_0 \mu_0 \frac{\partial \mathbf{E}}{\partial t} + \mu_0 \mathbf{J} \tag{6}$$

where the plasma current density is given by $\mathbf{J} = q_e\, n_{0e} \mathbf{u}_e$.

[24] The voltage at the antenna terminals is prescribed as the input to the simulation. A Gaussian derivative voltage pulse of sufficient spectral bandwidth is fed into the antenna structure. The resulting current at the feed point of the antenna is obtained from the simulation. The impedance of the antenna is then calculated by dividing the Fourier Transform of the Gaussian derivative voltage input by the Fourier Transform of the current through the antenna terminals. The PF-FDTD simulation is performed long enough so that at least 5 cycles of the lowest frequency of interest is captured.

[25] For the analysis performed here, the ambient electron density n_{0e}, electron neutral collision frequency ν_{en}, and electron cyclotron frequency f_{ce} are considered to be variable input parameters into the simulation. For a fixed set of parameters, the resulting impedance magnitude for the PF-FDTD simulation is shown in Figure 3 compared to the impedance magnitude of Balmain $Z_B(f)$. The minimum impedance is associated with the electron cyclotron resonance frequency f_{ce} and is referred to as the series resonance. At frequencies higher than f_{ce} the maximum impedance observed is associated with the upper hybrid resonant frequency f_{uh} and is called the parallel resonance.

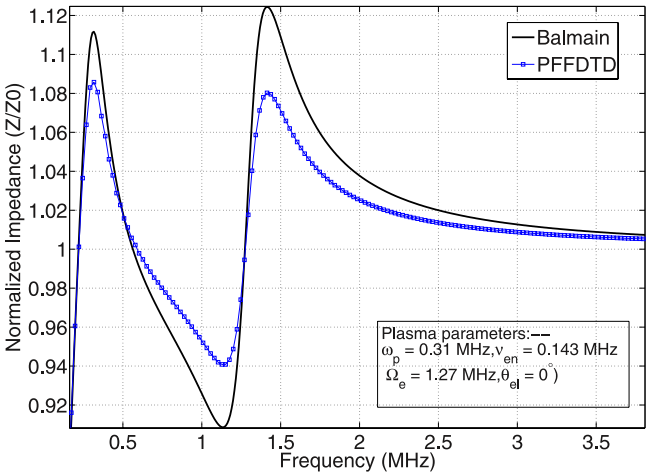

Figure 3. Simulated and theoretical plots of impedance magnitude of a dipole antenna of length of 1.04 m and diameter of 2.54 cm oriented along the magnetic field. Sheath size is assumed to be zero.

[26] We observe that the resonance positions predicted by the analytical formula $Z_B(f)$ are slightly shifted from that of the PF-FDTD simulation. This difference does not produce serious errors in the values of the parameters f_{pe} and f_{ce}. However, the PF-FDTD impedance curve $Z_{sim}(f)$ predicts a more damped response for the same value of ν_{en}. This difference makes the PF-FDTD a much more accurate tool to obtain the electron neutral collision frequency. For a match against data, PF-FDTD values of ν_{en} are at least 15–20% lower than the values obtained using the analytical formula.

5. Analysis of Impedance Data

[27] The analysis of the impedance data with the PF-FDTD simulation requires that initial estimates for the plasma parameters be determined. These initial parameters f_{pe}, f_{ce} and ν_{en} were determined by comparing the impedance magnitude data with the analytical formula $Z_B(f)$ using a least square fit algorithm weighted by the confidence level in the instrument measurement over different frequency ranges.

[28] With the starting parameters obtained from $Z_B(f)$, we performed simulation runs to compare the impedance magnitude curves produced by the PF-FDTD simulation $Z_{sim}(f)$ against the rocket impedance magnitude data $Z_m(f)$. The values were tuned until three alternative $Z_{sim}(f)$ fits were obtained to the measured impedance $Z_m(f)$. The three PF-FDTD matched results for each altitude, PF-1, PF-2 and PF-3, are chosen based on confidence in the measured impedance above the upper hybrid resonance frequency.

[29] PF-1 is chosen so that it approximates the lower envelope of the impedance magnitude data slope at frequencies higher than the upper hybrid resonance f_{uh}. PF-2 and PF-3 are chosen so that they approximate the median and the upper envelopes of the measured impedance slope at frequencies higher than the f_{uh}. This method for selection of the impedance curves is repeated for all upleg and downleg impedance data. This was done in order to get reasonable parameter values considering the uncertainty in the impedance data. The measured impedance curve is most reliable above f_{ce}. However, the data has some oscillation as the impedance magnitude curve decays after f_{uh}. Through our selection of upper, median and lower envelopes, we provide error bounds for values of the plasma parameters.

[30] For all the measurements the dipole was within the payload wake. The current was measured on only one arm of the dipole, which was always in a reasonably homogeneous plasma. *Barjatya and Swenson* [2006] have shown via a DSMC simulation that on the upleg the density around the SIP will see a minimum reduction by a factor of 1.25. However, the DSMC simulation includes only the neutral particles and a more substantive analysis of the wake structure involving the charged particle effects will be necessary in order to precisely account for the wake effects.

5.1. Upleg Analysis

[31] For the upleg, we selected three altitudes in the E_s layer. The three selected heights are 92.37 km, 92.41 km, and 92.44 km. The three altitudes are chosen to be at approximately the same height as those on the downleg. The horizontal rocket velocity was about 350 m/s and the distance between the selected locations is approximately 40 km. The SAL payload was at an angle of 68° with respect to the Earth's magnetic field on the upleg at the height of 92.5 km [*Gelinas*, 1999].

[32] The dipole was oriented perpendicular to the payload but the spin phase of the rocket could not be reliably determined. Since the angle of the dipole with respect to the magnetic field could vary between 22° to 90° on the upleg, all the simulation runs were done with an elevation angle (θ_{el}) equal to 22°, but the median envelope PF-2 curves were also matched using 90° elevation. This gives us the maximum spread of collision frequency values with the median envelope as a reference.

[33] At the altitude of 92.37 km, the PF-FDTD simulation best fits at elevation angle 22° are shown in Figure 4. The parameter values obtained are shown in Table 1,which also

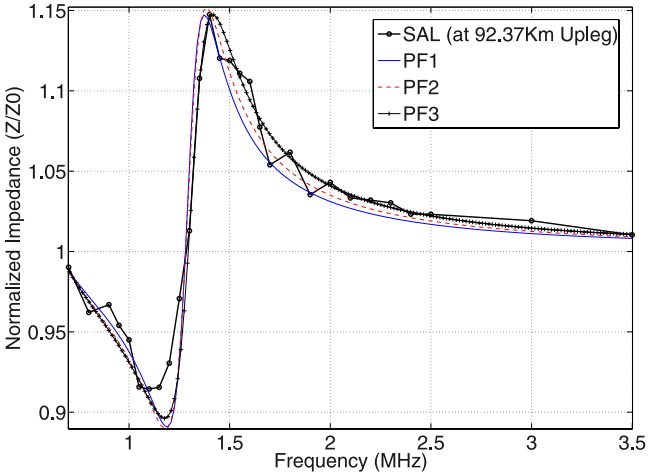

Figure 4. Three PF-FDTD impedance curves matched to SAL impedance data at an altitude of 92.37 km on the upleg.

Table 1. Plasma Parameters Obtained by Comparing SAL Impedance Data on the Upleg at an Elevation Angle θ_{el} 22° Against PF-FDTD Simulations and Balmain's Theory

Parameter	PF-1	PF-2	PF-3	Balmain
	Height = 92.37 km, Upleg			
ν_{en} (MHz)	0.09	0.10	0.12	0.15
n_{oe} (/cc)	1476	1658	1917	1552
B (nT)	46,355	46,355	46,852	46,374
	Height = 92.41 km, Upleg			
ν_{en} (MHz)	0.10	0.11	0.14	0.17
n_{oe} (/cc)	1658	1917	2343	1725
B (nT)	46,604	46,852	47,100	46,892
	Height = 92.44 km, Upleg			
ν_{en} (MHz)	0.11	0.12	0.14	0.17
n_{oe} (/cc)	1851	2125	2418	1914
B (nT)	46,604	46,604	47,352	46,666

shows plasma parameters obtained from Balmain's theory. The plasma parameters obtained from Balmain's model are obtained under the same matching condition as PF-2. We see that the plasma electron density n_{0e} increases from lower to upper envelopes, with the median envelope giving n_{0e} of 1658 cm^{-3}, which is between the lower and upper envelope n_{0e} values. The electron neutral collision frequency at this height is between 90 kHz to 120 kHz. The collision frequency values obtained from Balmain's theory are much higher than the values of PF-2.

[34] For the other two altitudes, we observe similar trends. The lowest plasma electron density (1476 cm^{-3}) was obtained at altitude 92.37 km and the highest (2418 cm^{-3}) at altitude 92.44 km. The impedance curves at 92.41 km and 92.44 km altitudes are shown in Figures 5 and 6 respectively.

[35] The cyclotron resonance troughs indicate a higher ambient magnetic field than that predicted by IGRF model. The IGRF model predicts a magnetic field of 38,706 nT which corresponds to a cyclotron frequency f_{ce} of 1.06 MHz. If this value is used in $Z_B(f)$ or the PF-FDTD analysis the resultant impedance curves cannot be matched to the measured data. Our analysis yields much higher values of

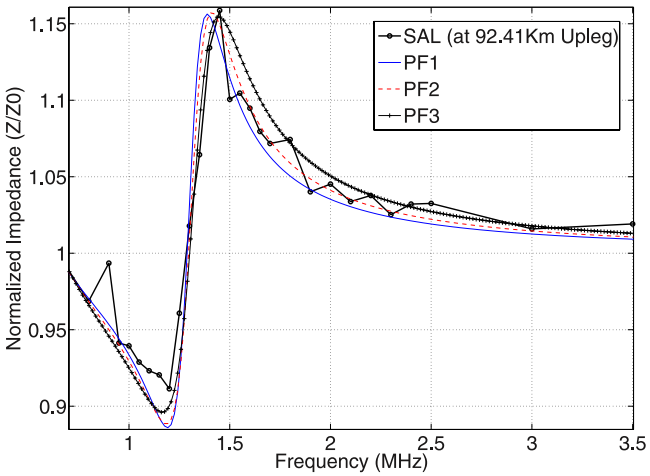

Figure 5. Three PF-FDTD impedance curves matched to SAL impedance data at an altitude of 92.41 km on the upleg.

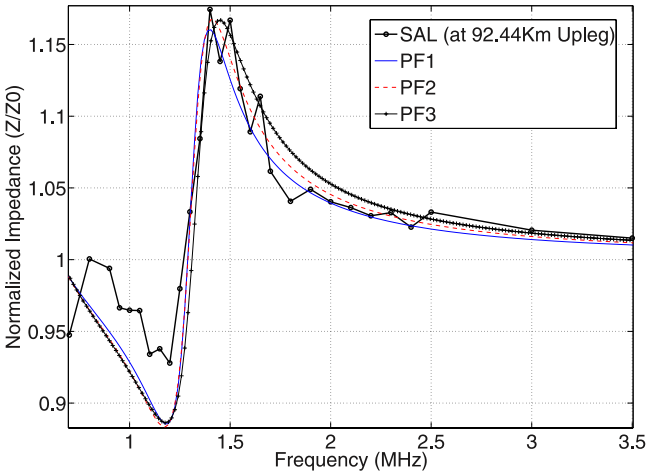

Figure 6. Three PF-FDTD impedance curves matched to SAL impedance data at an altitude of 92.44 km on the upleg.

ambient magnetic field strength between 46000 and 47000 nT. This may be due to an additional magnetic field from the Mass Spectrometer which was present on the payload.

[36] Over all three upleg altitudes, the collision frequencies ranged from 90 kHz (lowest value) at 92.38 km altitude to 140 kHz (highest value) at 92.41 km altitude. Using Balmain's theory for comparison against PF-2 yielded collision frequencies between 150 kHz and 170 kHz, while PF-2 values were between 101 kHz and 118 kHz.

5.2. Downleg Analysis

[37] The angle of the dipole with respect to the magnetic field varies between 72° to 90° on the downleg. All the simulation runs were done with an elevation angle (θ_{el}) equal to 72°, but the median envelope PF-2 curves were also matched using 90° elevation. This again gives us the maximum spread of collision frequency values with the PF-2 curve as a reference.

[38] The plasma parameters obtained with elevation angle 72° are shown in Table 2,which also shows plasma param-

Table 2. Plasma Parameters Obtained by Comparing SAL Impedance Data on the Downleg at an Elevation Angle θ_{el} 72° Against PF-FDTD Simulations and Balmain's Theory

Parameter	PF-1	PF-2	PF-3	Balmain
	Height = 92.38 km, Downleg			
ν_{en} (MHz)	0.07	0.10	0.09	0.16
n_{oe} (/cc)	944	1249	1476	1140
B (nT)	46,355	46,103	46,355	46,556
	Height = 92.41 km, Downleg			
ν_{en} (MHz)	0.11	0.14	0.16	0.18
n_{oe} (/cc)	1596	1986	2343	1430
B (nT)	46,852	46,355	46,604	46,764
	Height = 92.44 km, Downleg			
ν_{en} (MHz)	0.11	0.12	0.13	0.17
n_{oe} (/cc)	2270	2494	2729	1730
B (nT)	46,604	47,352	47,849	47,615

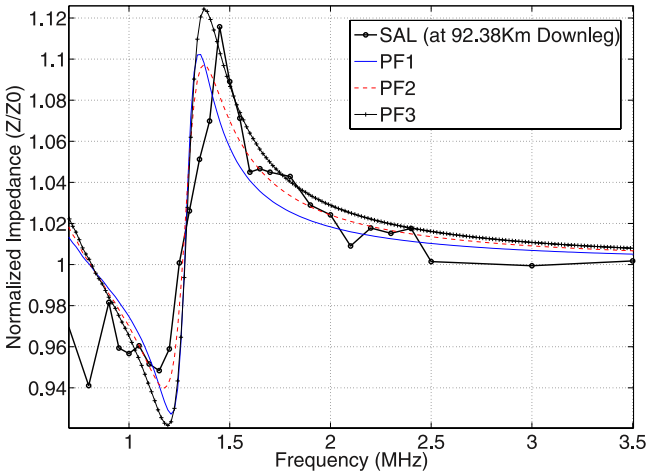

Figure 7. Three PF-FDTD impedance curves matched to SAL impedance data at an altitude of 92.38 km on the downleg.

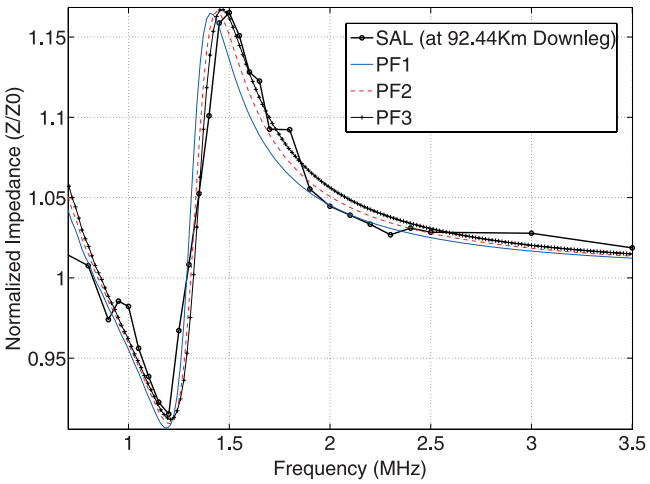

Figure 9. Three PF-FDTD impedance curves matched to SAL impedance data at an altitude of 92.45 km on the downleg.

eters obtained from Balmain's theory. We note that the ambient magnetic field strengths obtained on the downleg were again much higher than predicted by the IGRF model.

[39] For the downleg altitude of 92.38 km, 92.41 km and 92.44 km the PF-FDTD simulation results are shown in Figures 7, 8 and 9. As was observed on the upleg, the plasma electron density n_{0e} increases from lower to upper envelopes, with the median envelope giving n_{0e} of 1249 cm^{-3}, which is between the lower and upper envelope n_{0e} values. The electron neutral collision frequency at this height is between 68 kHz to 100 kHz. Higher values of collision frequency are again predicted by Balmain's model when compared with PF-2.

[40] The lowest plasma electron density of 944 cm^{-3} was obtained at altitude 92.38 km and the highest value 2729 cm^{-3} at altitude 92.45 km. Collision frequencies varied from a low of 70 kHz at 92.38 km to a high of 160 kHz at 92.41 km. PF-2 collision frequency values varied between 100 kHz and 138 kHz, Balmain's theory in comparison yielded collision frequencies between 156 kHz and 180 kHz.

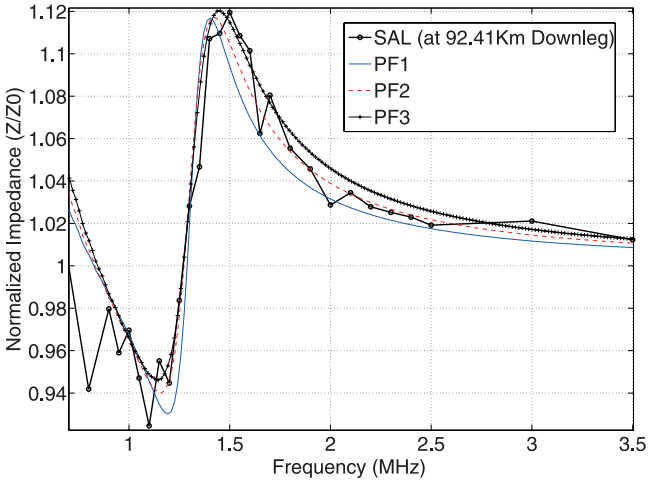

Figure 8. Three PF-FDTD impedance curves matched to SAL impedance data at an altitude of 92.41 km on the downleg.

6. Discussion

[41] For a cold collisional fluid plasma the flow of the electrons perpendicular to the magnetic field is given by *Cowley* [2000],

$$\mathbf{u}_{\mathbf{e}\perp} = \frac{1}{1+\left(\frac{\nu_{en}}{2\pi f_{ce}}\right)^2}\left[\frac{\mathbf{E}\times\mathbf{B}}{B^2} - \frac{\nu_{en}}{2\pi f_{ce}}\frac{\mathbf{E}_\perp}{B}\right] \tag{7}$$

[42] Under the same assumptions the field-perpendicular ion flow will have a similar expression. If the ambient density of ions (n_{0i}) is assumed equal to n_{0e} then the current density perpendicular to the magnetic field is given by,

$$\begin{aligned} j_\perp &= n_{0e}e(\mathbf{u}_{\mathbf{i}_\perp} - \mathbf{u}_{\mathbf{e}_\perp}) \\ &= \sigma_p\mathbf{E} + \sigma_H\mathbf{B}\times\mathbf{E} \end{aligned} \tag{8}$$

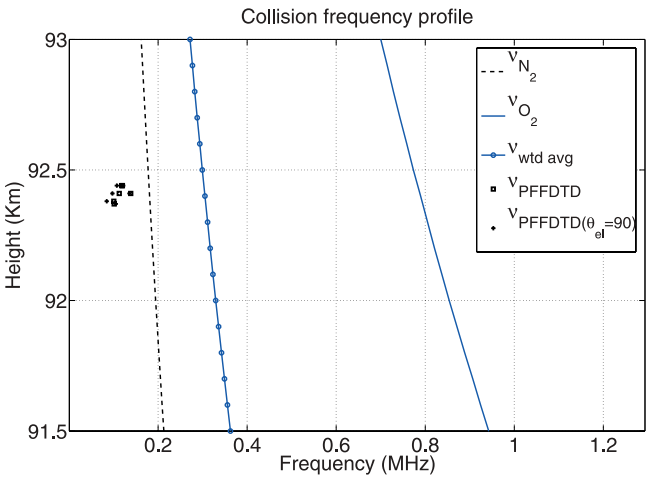

Figure 10. Collision frequencies inferred from PF-FDTD best fits to SAL PIP data plotted along with the theoretical values obtained from *Schunk and Nagy* [2000].

where $\mathbf{u}_{i\perp}$ is the field-perpendicular ion flow velocity, σ_p and σ_H are the Pederson and Hall conductivity. The ratio ν_{en}/f_{ce} is expected to remain small throughout the whole region of the ionosphere where appreciable plasma densities are present (above ~90 km). Thus electrons should $\mathbf{E} \times \mathbf{B}$ drift at all ionospheric altitudes and contribute only to the Hall current [*Cowley*, 2000]. Further, electron drift along neutral winds is negligible at altitudes between 80–100 km [*Heelis*, 2004].

[43] Electron neutral collisions at 90–100 km are dominated by momentum transfer mechanisms [*Schunk and Nagy*, 2000]. At an altitude of around 92–95 km the momentum transfer collision frequencies calculated from the Chapman-Cowling collision integral [*Chapman and Cowling*, 1970] depend strongly on the density of molecular nitrogen (N_2) and oxygen (O_2).

[44] The electron-oxygen and electron-nitrogen collision frequencies with changing density and electron temperature are given by *Schunk and Nagy* [2000],

$$\nu_{N_2} = 2.33 \times 10^{-11} n_{N_2} \left(1 - 1.21 \times 10^{-4} T_e\right) T_e \tag{9}$$

$$\nu_{O_2} = 1.82 \times 10^{-10} n_{O_2} \left(1 + 3.6 \times 10^{-2} \sqrt{T_e}\right) \sqrt{T_e} \tag{10}$$

where n_{N_2} and n_{O_2} are the molecular nitrogen and oxygen densities respectively.

[45] We obtain the neutral densities and the electron temperature profiles from the MSISE-90 model, the inputs being the day, time, year, latitude and longitude of the SAL mission. The MSISE values are then used in equations (9) and (10) to produce an altitude profile for the collision frequencies. To obtain the effective electron neutral collision frequency with altitude, we calculate the weighted average of the two collision frequency profiles according to the expression,

$$\nu_{avg} = \frac{n_{N_2}\nu_{N_2} + n_{O_2}\nu_{O_2}}{n_{N_2} + n_{O_2}} \tag{11}$$

[46] When the densities of the neutral species are almost equal, the weighted average drops down to the arithmetic mean of the two collision frequencies [*Chau and Kudeki*, 2006]. The altitude profiles generated for electron-nitrogen, electron-oxygen and weighted average collision frequencies are shown in Figure 10. The collision frequency values obtained from the median envelopes (PF-2) are also shown in Figure 10. In addition to the values obtained for the upleg and downleg angles of 22 and 72 degrees, we also show the values obtained with the maximum 90 degree elevation between the dipole and ambient magnetic field. We observe that the collision frequencies using the median envelope (22 and 90 degrees upleg, 72 and 90 degrees downleg) are all within 10 percent of each other at each altitude.

[47] The highest and lowest values obtained from PF-FDTD analysis for the ratio of ν_{en} to f_{ce} (1.06 MHz, obtained from IGRF) are 0.066 and 0.1509 respectively. These numbers are consistent with the assumption that electrons contribute only to the Hall current. We also note that the electron neutral collision frequencies obtained from the PF-FDTD simulation are lower than the collision frequencies derived from the quiet time MSISE-90 neutral densities.

7. Conclusions and Future Work

[48] We found that a Swept Impedance Probe can be used to measure the electron neutral collision frequency and electron density accurately in the vicinity of the probe. The PF-FDTD simulation is a much more powerful tool to estimate the electron fluid parameters than the analytical formulas of Balmain. This is especially true in the case of values of ν_{en}. The electron neutral collision frequency values obtained were more than 20% lower than the values predicted by Balmain's theory.

[49] Since the dipole was within the wake structure of the payload when the measurements were made, a correction factor needs to be determined to obtain the true values of n_{0e} and ν_{en} far away from the payload. In order to do this a more substantive analysis of the wake structure involving the charged particle effects will be necessary. We are currently researching the available techniques to perform this analysis.

[50] Simulation time limits the usage of PF-FDTD to analyzing relatively small data sets. Future work will continue to reduce the simulation time by efficient utilization of memory allocation and paralleling the finite difference calculations. This will allow the simulation to be used for analyzing the impedance over the entire flight path.

[51] **Acknowledgments.** The authors wish to thank Wayne G. Sanderson from the Space Dynamics laboratory for many helpful discussions on the working of the SIP instrument.

[52] Zuyin Pu thanks Lynette Gelinas and another reviewer for their assistance in evaluating this paper.

References

Balmain, K. (1964), The impedance of a short dipole antenna in a magnetoplasma, *IEEE Trans. Antennas Propag.*, *12*(5), 605–617.

Balmain, K. (1969), Dipole admittance for magnetoplasma diagnostics, *IEEE Trans. Antennas Propag.*, *17*(3), 389–392.

Balmain, K. (1979), The properties of antennas in plasmas, *Ann. Telecommun.*, *34*, 273–283.

Barjatya, A., and C. Swenson (2006), Observation of triboelectric charging effects on Langmuir-type probes in dusty plasma, *J. Geophys. Res.*, *111*, A10302, doi:10.1029/2006JA011806.

Bishop, R., and K. Baker (1972), Electron temperature and density determination from RF impedance probe measurements in the lower ionosphere, *Planet. Space Sci.*, *20*, 997–1013.

Blackwell, D., D. Walker, S. Messer, and W. Amatucci (2005a), Characteristics of the plasma impedance probe with constant bias, *Phys. Plasmas*, *12*(093510).

Blackwell, D. D., D. N. Walker, and W. E. Amatucci (2005b), Measurement of absolute electron density with a plasma impedance probe, *Rev. Sci. Instrum.*, *76*(023503).

Blackwell, D., D. Walker, S. Messer, and W. Amatucci (2007), Antenna impedance measurements in a magnetized plasma. II: Dipole antenna, *Phys. Plasmas*, *14*(092106).

Carlson, C. G. (2004), Next generation plasma frequency probe instrumentation technique, Master's thesis, Utah State Univ., Logan, Utah.

Carlson, C. G., C. M. Swenson, and C. Fish (2003), Next generation plasma impedance probe instrumentation technique, *AGU Fall Meeting*, Abstracts SA12B-1106.

Chapman, S., and T. G. Cowling (1970), *The Mathematical Theory of Nonuniform Gases*, Cambridge Univ. Press, New York.

Chau, J. L., and E. Kudeki (2006), First e- and d-region incoherent scatter spectra observed over Jicamarca, *Ann. Geophys.*, *24*, 1295–1303.

Cowley, S. W. H. (2000), TUTORIAL: Magnetosphere-ionosphere interactions: A tutorial review, in *Magnetospheric Current Systems*, *Geophys. Monogr. 118*, pp. 91+, AGU, Washington, D. C.

Gelinas, L. J. (1999), An in-situ measurement of charged mesospheric dust during a sporadic a sporadic atom layer event, Ph.D. thesis, Univ. of New Hampshire, Durham, N. H.

Heelis, R. (2004), Electrodynamics in the low and middle latitude ionosphere: A tutorial, *J. Atmos. Sol.-Terr. Phys.*, *66*, 825–838.

Nikitin, P., and C. Swenson (2001), Impedance of a short dipole antenna in a cold plasma, *IEEE Trans. Antennas Propag.*, *49*(10), 1377–1381.

Oliver, B., R. Clements, and P. Smy (1973), Experimental investigation of the low-frequency capacitive response of a plasma sheath, *J. Appl. Phys.*, *44*, 4511–4517.

Rao, B. R., and B. Bhat (1969), Experimental investigation on the impedance behavior of a short, cylindrical antenna in a lossy magnetoplasma, *NASA Tech. Rep. Server, NASA-CR-107453, SR-2*, Harvard Univ., Cambridge, Mass.

Rowland, D. E., R. F. Pfaff, P. Uribe, and J. Burchill (2006), Plasma impedance spectrum analyzer (PISA): An advanced impedance probe for measuring plasma density and other parameters, *AGU Fall Meeting*, Abstracts SM12A-07, San Francisco.

Sawaya, K., T. Ishizone, and Y. Mushiake (1978), Measurement of the impedance of a linear antenna in a magnetoplasma, *Radio Sci.*, *13*(1), 21–29.

Schunk, R. W., and A. F. Nagy (2000), *Ionospheres, Physics, Plasma Physics, and Chemisty*, *Cambridge Atmospheric and Space Science Series*, Cambridge Univ. Press, New York.

Staras, H. (1964), The impedance of an electric dipole in a magneto-ionic medium, *IEEE Trans. Antennas Propag.*, *12*, 695–702.

Taflove, A., and S. Hagness (2005), *Computational Electrodynamics: The Finite-Difference Time-Domain Method*, Artech House, London, U.K.

Ward, J. (2006), The numerical modelling of an antenna in plasma, Ph.D. thesis, Utah State University, Logan, Utah.

Ward, J., C. Swenson, and C. Furse (2005), The impedance of a short dipole antenna in a magnetized plasma via a finite difference time domain model, *IEEE Trans. Antennas Propag.*, *53*(8), 2711–2718.

Yee, (1966), Numerical solution of initial boundary value problems involving Maxwell's equations in isotropic media, *IEEE Trans. Antennas Propag.*, *14*(3), 302–307.

T. Andriyas, S. Patra, E. Spencer, and C. Swenson, Center for Space Engineering, 4170 Old Main Hill, Logan, UT 84322, USA. (espencer@engineering.usu.edu)

A. Barjatya, Physical Sciences Department, Embry-Riddle Aeronautical University, 600 South Clyde Morris Boulevard, Daytona Beach, FL 32114, USA.

J. Ward, Computer and Electronics Engineering Technology, Weber State University, 1703 University Circle, Ogden, UT 84408-1703, USA.